LETTERS

(π, π) electronic order in iron arsenide superconductors

V. B. Zabolotnyy[1], D. S. Inosov[1,2], D. V. Evtushinsky[1], A. Koitzsch[1], A. A. Kordyuk[1,3], G. L. Sun[2], J. T. Park[2], D. Haug[2], V. Hinkov[2], A. V. Boris[2,4], C. T. Lin[2], M. Knupfer[1], A. N. Yaresko[2], B. Büchner[1], A. Varykhalov[5], R. Follath[5] & S. V. Borisenko[1]

The distribution of valence electrons in metals usually follows the symmetry of the underlying ionic lattice. Modulations of this distribution often occur when those electrons are not stable with respect to a new electronic order, such as spin or charge density waves. Electron density waves have been observed in many families of superconductors[1–3], and are often considered to be essential for superconductivity to exist[4]. Recent measurements[5–9] seem to show that the properties of the iron pnictides[10,11] are in good agreement with band structure calculations that do not include additional ordering, implying no relation between density waves and superconductivity in these materials[12–15]. Here we report that the electronic structure of $Ba_{1-x}K_xFe_2As_2$ is in sharp disagreement with those band structure calculations[12–15], and instead reveals a reconstruction characterized by a (π, π) wavevector. This electronic order coexists with superconductivity and persists up to room temperature (300 K).

Calculations of the electronic structure of the new pnictide superconductors unanimously predict a Fermi surface consisting of a hole-like pocket at the centre (Γ point) of the Brillouin zone and electron-like ones at the corners (X points) of the Brillouin zone. A shift by a (π, π) vector would result in a significant overlap of these Fermi surfaces. Such an electronic structure is highly unstable because any interaction allowing an electron to gain a (π, π) momentum would favour a density-wave order, resulting in a shift of the aforementioned type and a concomitant opening of the gaps, thus strongly reducing the electronic kinetic energy. It is surprising that angle-resolved photoemission spectroscopy (ARPES) data are reported to be in general, and sometimes in very detailed[9], agreement with calculations that give a potentially unstable solution[5–7]. Even in the parent compound, where the spin-density-wave transition is clearly seen using other techniques[16,17], no evidence for the expected energy gap has been detected in photoemission experiments[7,8]. In fact, no consensus exists regarding the overall Fermi surface topology. According to refs 5 and 6, there is a single electron-like Fermi surface pocket around X, whereas ref. 18 reported two intensity spots without any discernible signature for the electron pocket in the normal state. Intensity spots near X were also reported in refs. 6, 7 and 9, but those are interpreted as parts of electron-like pockets. Such substantial variations in the photoemission signal preclude unambiguous assignment of the observed features to the calculated Fermi surface, leaving the electronic structure of the arsenides unclear.

In Fig. 1, we show the experimental Fermi surface map of $Ba_{1-x}K_xFe_2As_2$ (BKFA) measured in the superconducting state. To eliminate possible effects of photoemission matrix elements, as well as to cut the electronic structure at different values of momentum, k_z, we made measurements at several excitation energies (Fig. 1a, b) and polarizations (Fig. 1c, d). Although there are obvious changes in the intensities of the features, no signatures indicating k_z dispersion can be conclusively identified. With this in mind, the apparently different intensity distributions at neighbouring Γ points appear unusual. In the first Brillouin zone, the two concentric contours are broadly consistent with band structure calculations, but the 'design wheels' centred at the Γ points (Fig. 1a, b) in the second Brillouin zone are at variance with predicted hole-like circles. The major discrepancy with theoretical calculations and ARPES data[5–9,18] is observed near X, where, according to the calculations, a sizeable double-walled electron pocket is expected. Instead, we observe a propeller-shaped structure consisting of five small Fermi surface sheets: a pocket, situated directly at X, and four 'blades' surrounding it. Fig 1c, d shows that these Fermi surfaces are not only well separated but also have different symmetries.

To examine the topology of these five pockets, we look at the momentum distribution of intensity below and above the Fermi level. As can be seen in Fig. 2a–c, the size of the X-centred pocket

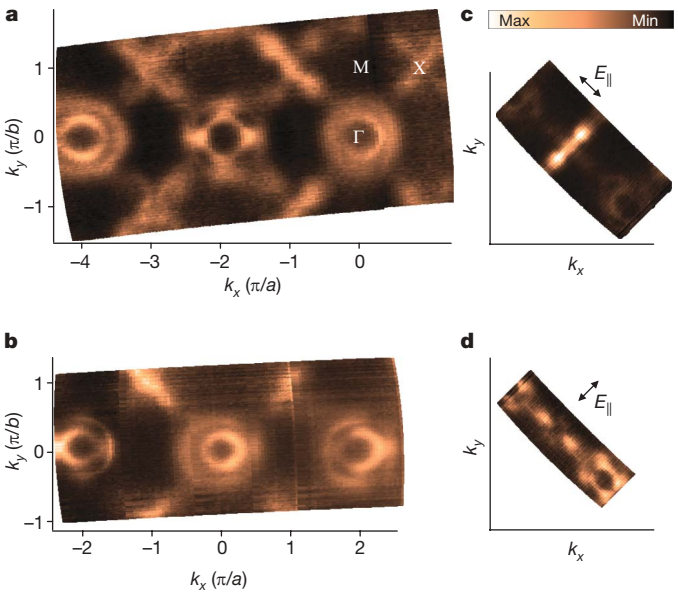

Figure 1 | Fermi surface topology of $Ba_{1-x}K_xFe_2As_2$. The colour plots display the photoelectron intensity distribution as a function of quasi-momentum, $k_\parallel$, integrated over a small energy window of 15 meV around the Fermi level. **a**, **b**, Fermi surface maps of $Ba_{1-x}K_xFe_2As_2$ measured using respective excitation energies of $h\nu = 80$ and 50 eV at $T = 14$ K (here ν denotes frequency and h denotes Planck's constant). **c**, **d**, These images, measured at $h\nu = 80$ eV, demonstrate the strong effect of light polarization on the photoemission from the four small Fermi surfaces surrounding X. The component of the electric field parallel to the sample surface, $E_\parallel$, is indicated by a double-headed arrow. Experimental details concerning the sample preparation can be found in Supplementary Information. *a*, *b*, lattice parameters.

[1]Institute for Solid State Research, IFW-Dresden, PO Box 270116, 01171 Dresden, Germany. [2]Max-Planck-Institute for Solid State Research, Heisenbergstrasse 1, 70569 Stuttgart, Germany. [3]Institute of Metal Physics of National Academy of Sciences of Ukraine, 03142 Kyiv, Ukraine. [4]Department of Physics, Loughborough University, Loughborough, LE11 3TU, UK. [5]Elektronenspeicherring BESSY II, Helmholtz-Zentrum Berlin für Materialien und Energie, Albert-Einstein-Strasse 15, 12489 Berlin, Germany.

clearly increases when the electronic structure is cut above the Fermi level, and decreases when the cut is made below the Fermi level, which confirms its electron-like topology. On the other hand, the blades surrounding X have the opposite behaviour, which shows that they are hole-like. In Fig. 2e–i, we analyse the band dispersions along the cuts given in Fig. 2d, and again find support for these conclusions (see also Supplementary Information). Therefore, the observed topology of the Fermi surface is different from that predicted by band structure calculations. However, in the following we will argue that the results of the calculations can be reconciled with the experimental data, provided the system reacts to the predicted nesting instability and an ordered state develops.

In Fig. 3, we collate the ARPES data taken at low temperatures for the parent compound with the spectra of the doped superconductor, measured using the same light polarization as in Fig. 1d. The photoemission intensity distributions shown in Fig. 3a, b are comparable when the difference in the charge carrier concentrations is taken into account. Moreover, the momentum–energy cuts (Fig. 3c–h) show that there is a one-to-one correspondence between the underlying band dispersions in the parent and superconducting samples. Similar locations in the momentum–energy space, as well as the characteristic, polarization-induced intensity variations, clearly suggest that the blades are also present in $BaFe_2As_2$ (BFA). Notably, the distance between the centres of opposite blades tracks the size of the Γ-Fermi surface. Closer inspection of all existing ARPES data on arsenides confirms the universality of this observation[6–9,18].

The origin of the unexpected Fermi surface topology near X is clarified in Fig. 3i, j, where momentum–energy cuts separated by the (π, π) vector are shown: the blades in the parent compound are created by the interaction of the (π, π) replica of the Γ-centred Fermi surface with the X-centred electron-like Fermi surface predicted in the calculations. Such a (π, π) folding implies the presence of additional ordering that sets in to relax the nesting instability. The formation of the blades, within this picture, is illustrated by simple sketch in Fig. 3k. The intensity of the Γ-derived band in Fig. 3j is lower than that shown in Fig. 3j owing to the weakness, relative to the original crystalline potential, of the scattering potential introduced by the new order[19,20]. This is also the case for the Fermi surface map in Fig. 3a, where the ARPES intensities near Γ and X still differ. Similarly, in superconducting BKFA this effect prevents immediate detection of the ordered state suggested by the blades. By recovering the band dispersion in the vicinity of the Fermi level, as shown in Fig. 3l–m, we can identify new Brillouin zone boundaries (white lines).

An immediate interpretation of the observed similarity in the electronic structures of the $x = 0.0$ and $x = 0.3$ compounds shown in Fig. 3 would be the persistence of magnetic order in the superconducting case, which does not contradict the phase diagram suggested in ref. 21. However, the temperature evolution of the photoemission intensity of the blades presented in Fig. 4b rules out any direct connection between the observed Fermi surface topology and the static magnetic order. Despite the blades having a noticeably lower spectral weight in comparison with the Γ-Fermi surface sheets, these hole-like structures clearly persist to room temperature (Fig. 4a), which is above the structural, magnetic and superconducting transitions in arsenides. Such temperature behaviour also rules out the possibility that the observed Fermi surface topology near the X points is a consequence of a pronounced deformation of the calculated band structure, which would destroy the Fermi surface nesting. To account

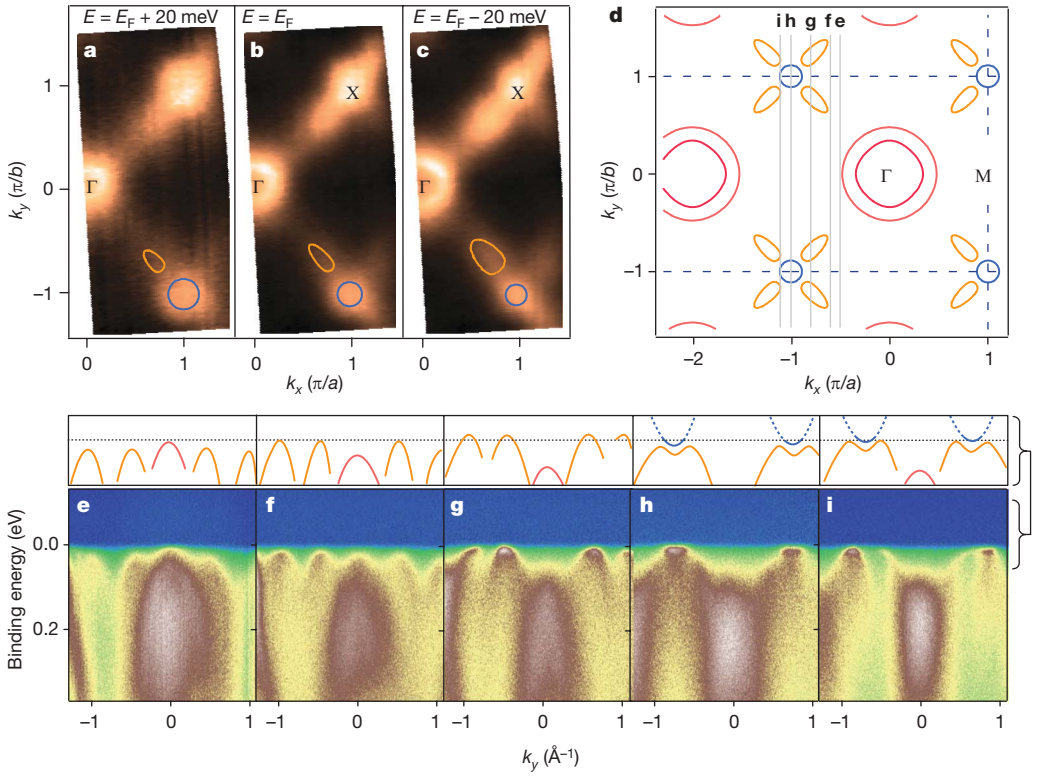

Figure 2 | Low-energy electronic structure of $Ba_{1-x}K_xFe_2As_2$. **a–c**, Momentum dependence of the photoemission intensity at constant-energy cuts for $Ba_{1-x}K_xFe_2As_2$ ($T = 150$ K, $h\nu = 70$ eV). The size of the blade pockets (outlined by the orange lines) increases with cut energy, E, and signals their hole-like topology. The opposite trend for the X-centred pocket (blue circles) implies the electron-like topology of that pocket. To avoid obscuring the experimental data, we display the guide lines only in the lower parts of the images. E_F, Fermi energy. **d**, Summary of the derived Fermi surface topology. **e–i**, Energy–momentum cuts showing low-energy band dispersions ($T \leq 15$ K, $h\nu = 80$ eV). The cartoon above each image outlines the band dispersions and the formation of the hole and electron pockets at the Fermi level. In cut **e**, five parabolic bands with similar dispersions can be seen approaching, but not crossing, the Fermi level. With movement away from Γ (cuts **f–g**), the four bands on the sides finally cross the Fermi level, forming the blade structure near the X points. However, when the cut passes directly through the X points (cut **h**), these four hole-like bands again drop below the Fermi level, and instead two electron-like bands, of curvature opposite to that of the previous bands, appear from above the Fermi level.

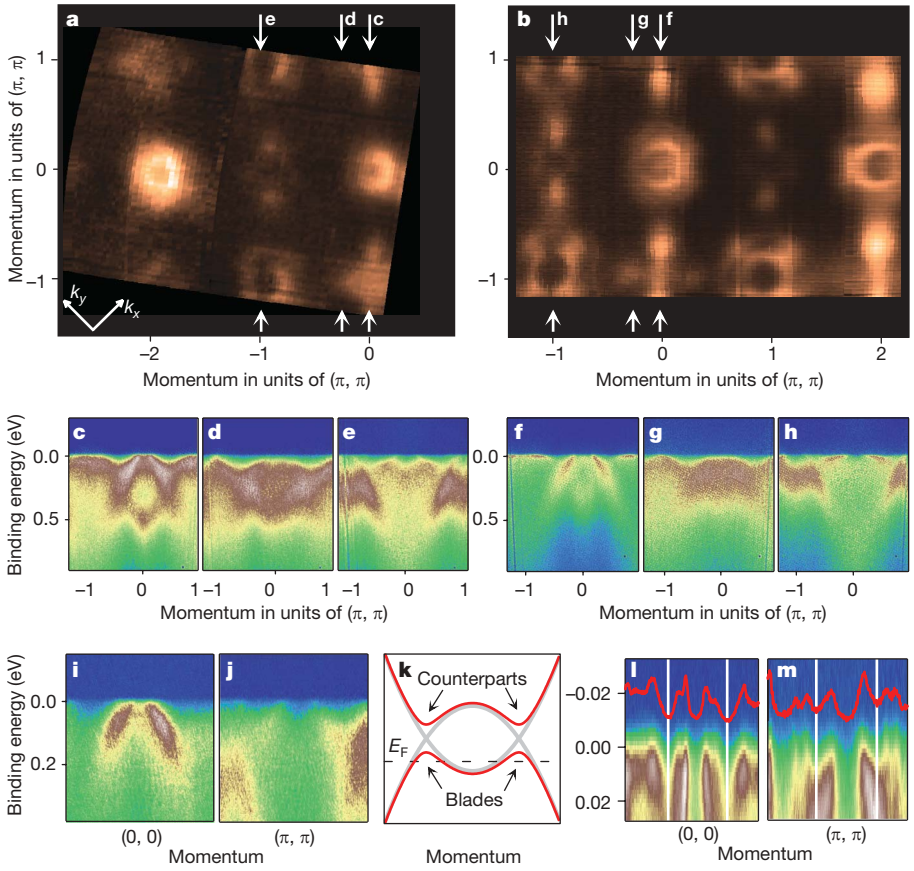

Figure 3 | (π, π) reconstruction of the electronic structure. **a**, **b**, Fermi surface maps for BFA and BKFA, respectively ($h\nu = 80$ eV). **c**–**h**, Several typical energy–momentum cuts, normalized to integrated intensity, showing similar band dispersions for BFA (**c**, **d**, **e**) and BKFA (**f**, **g**, **h**). The cut positions in momentum space are indicated by the arrows in **a** and **b**. **i**, **j**, Parallel cuts through the electronic structure of BFA, set apart by the (π, π) vector. **k**, Simplest model showing the result of folding of single hole- and electron-like bands. **l**, **m**, Parallel cuts through Γ and X in the electronic structure of BKFA, set apart by the (π, π) vector. Red curves are the momentum distribution curves integrated within the 8-meV-wide energy window, showing the symmetric behaviour about the new Brillouin zone boundaries (white lines) due to (π, π) folding of the original structure.

for the observed hole-like structures, some of bands at X would have to be shifted by 250 meV (refs 5, 13–15), which is not likely to occur. In addition, the potential candidates to form the hole and electron pockets at X do not interact, for reasons of symmetry, and thus would not be able to account for the picture shown in Fig. 3k (Supplementary Information).

Our ARPES data manifest the presence of electronic order of a special kind. This order sets in at high temperatures and is dictated by the nesting instability predicted in the calculations. Most likely it is this electronic order that results in the structural transition at lower temperatures in the parent compound, as in the case of $La[O_{1-x}F_x]FeAs$ the static magnetic order develops only after the structural transition and magnetic moments are much smaller than theoretically expected[16,17]. On the other hand, presence of the (π, π) excitations (wavevector, $q = 1.15$ Å^{-1}) above the superconducting transition is implied by the inelastic neutron scattering data[22], and their transformation into a resonance below the critical temperature (T_c) could indicate their crucial role in the mechanism of superconductivity. If these excitations correspond to a fluctuating stripe-like order, the propeller structure could result from a superposition of two pairs of blades originating from folding associated with (π, π) and (π, −π) wavevectors.

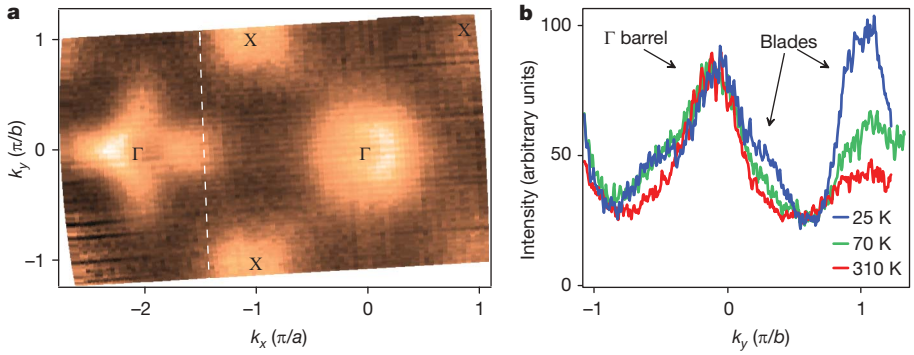

Figure 4 | Blade structure at X. **a**, Fermi surface map measured at $T = 300$ K ($h\nu = 50$ eV), demonstrating persistence of the blade-related intensity to high temperatures. **b**, Temperature dependence of the blade intensity compared with that of the Γ barrel. The plot represents the intensity along the cut shown in **a** (dashed line) and was integrated in the 100-meV window centred on the Fermi level.

The observed order is not a conventional charge density wave, as the atoms respond only at considerably lower temperatures[16,17]; but because the low-lying electronic structure is formed exclusively by the *d* electrons, it may be related to a more complex order parameter, as in the case of the hidden-order picture suggested for the cuprates[4]. Observation of the reconstruction below T_c implies the coexistence of the (π, π) order and the superconductivity, which is confirmed by opening of the superconducting gaps on the 'propeller' Fermi surface[23]. The order weakens with doping, which may explain why it is no longer strong enough to cause the structural transition and/or static magnetism, but is sufficient to open smaller (π, π) gaps near X, thus providing a high density of states at the Fermi level that might be necessary for superconductivity[24].

Received 11 September; accepted 2 December 2008.

1. Wise, W. D. *et al.* Charge-density-wave origin of cuprate checkerboard visualized by scanning tunnelling microscopy. *Nature Phys.* **4,** 696–699 (2008).
2. Kawasaki, S. *et al.* Enhancing the superconducting transition temperature of $CeRh_{1-x}Ir_xIn_5$ due to the strong-coupling effects of antiferromagnetic spin fluctuations: an ^{115}In nuclear quadrupole resonance study. *Phys. Rev. Lett.* **96,** 147001 (2006).
3. Morosan, E. *et al.* Superconductivity in Cu_xTiSe_2. *Nature Phys.* **2,** 544–550 (2006).
4. Chakravarty, S. *et al.* Hidden order in the cuprates. *Phys. Rev. B* **63,** 094503 (2001).
5. Liu, C. *et al.* K-doping dependence of the Fermi surface of the iron-arsenic $Ba_{1-x}K_xFe_2As_2$ superconductor using angle-resolved photoemission spectroscopy. *Phys. Rev. Lett.* **101,** 177005 (2008).
6. Ding, H. *et al.* Observation of Fermi-surface-dependent nodeless superconducting gaps in $Ba_{0.6}K_{0.4}Fe_2As_2$. *Europhys. Lett.* **83,** 47001 (2008).
7. Zhang, Y. *et al.* Correlation effects of exchange splitting and coexistence of spin-density-wave and superconductivity in single crystalline $Sr_{1-x}K_xFe_2As_2$. Preprint at ⟨http://arxiv.org/abs/0808.2738v1⟩ (2008).
8. Yang, L. X. *et al.* Electronic structure and exotic exchange splitting in spin-density-wave states of $BaFe_2As_2$. Preprint at ⟨http://arxiv.org/abs/0806.2627v2⟩ (2008).
9. Lu, D. H. *et al.* Electronic structure of the iron-based superconductor LaOFeP. *Nature* **455,** 81–84 (2008).
10. Chen, X. H., Wu, T., Wu, G., Liu, R. H. & Fang, D. F. Superconductivity at 43 K in $SmFeAsO_{1-x}F_x$. *Nature* **453,** 761–762 (2008).
11. Kamihara, Y., Watanabe, T., Hirano, M. & Hosono, H. Iron-based layered superconductor $La[O_{1-x}F_x]FeAs$ ($x = 0.05 - 0.12$) with $T_C = 26$ K. *J. Am. Chem. Soc.* **130,** 3296–3297 (2008).
12. Singh, D. J. Electronic structure and doping in $BaFe_2As_2$ and LiFeAs: density functional calculations. Preprint at ⟨http://arxiv.org/abs/0807.2643v1⟩ (2008).
13. Ma, F., Lu, Z.-Y. & Xiang, T. Electronic band structure of $BaFe_2As_2$. Preprint at ⟨http://arxiv.org/abs/0806.3526v1⟩ (2008).
14. Nekrasov, I. A., Pchelkina, Z. V. & Sadovskii, M. V. Electronic structure of prototype AFe_2As_2 and ReOFeAs high-temperature superconductors: a comparison. *JETP Lett.* **88,** 155–160 (2008).
15. Mazin, I. I., Singh, D. J., Johannes, M. D. & Du, M. H. Unconventional sign-reversing superconductivity in $LaFeAsO_{1-x}F_x$. *Phys. Rev. Lett.* **101,** 057003 (2008).
16. de la Cruz, C. *et al.* Magnetic order close to superconductivity in the iron-based layered $LaO_{1-x}F_xFeAs$ systems. *Nature* **453,** 899–902 (2008).
17. Huang, Q. *et al.* Neutron-diffraction measurements of magnetic order and a structural transition in the parent $BaFe_2As_2$ compound of FeAs-based high-temperature superconductors. *Phys. Rev. Lett.* **101,** 257003 (2008).
18. Zhao, L, *et al.* Multiple nodeless superconducting gaps in $(Ba_{0.6}K_{0.4})Fe_2As_2$ superconductor from angle-resolved photoemission spectroscopy. *Chin. Phys. Lett.* **25,** 4402–4405 (2008).
19. Brouet, V. *et al.* Angle-resolved photoemission study of the evolution of band structure and charge density wave properties in RTe_3 (R=Y, La, Ce, Sm, Gd, Tb, and Dy). *Phys. Rev. B* **77,** 235104 (2008).
20. Borisenko, S. V. *et al.* Pseudogap and charge density waves in two dimensions. *Phys. Rev. Lett.* **100,** 196402 (2008).
21. Chen, H. *et al.* Coexistence of the spin-density-wave and superconductiviy in the $Ba_{1-x}K_xFe_2As_2$. *Europhys. Lett.* **85,** 17006 (2009).
22. Christianson, A. D. *et al.* Resonant spin excitation in the high temperature superconductor $Ba_{0.6}K_{0.4}Fe_2As_2$. Preprint at ⟨http://arxiv.org/abs/0807.3932v1⟩ (2008).
23. Evtushinky, D. V. *et al.* Momentum dependence of the superconducting gap in $Ba_{1-x}K_xFe_2As_2$. Preprint at ⟨http://arxiv.org/abs/0809.4455v1⟩ (2008).
24. Radtke, R. J. & Norman, M. R. Relation of extended Van Hove singularities to high temperature superconductivity within strong-coupling theory. *Phys. Rev. B* **50,** 9554–9560 (1994).

Supplementary Information is linked to the online version of the paper at www.nature.com/nature.

Acknowledgements The project was supported, in part, by the Deutsche Forschungsgemeinschaft under grant numbers KN393/4 and BO 1912/2-1. We are grateful to I. Eremin, O. K. Andersen, L. Boeri, I. Mazin and M. Rümelli for discussions. We thank R. Hübel for technical support.

Author Information Reprints and permissions information is available at www.nature.com/reprints. Correspondence and requests for materials should be addressed to S.V.B. (s.borisenko@ifw-dresden.de).